Infrared reflectivity and Raman intensity spectrum of relaxor ferroelectric $Na_{1/2}Bi_{1/2}TiO_3$ at room temperature: a first-principles theoretical study

Materials Research Express

Infrared reflectivity and Raman intensity spectrum of relaxor ferroelectric Na$_{1/2}$Bi$_{1/2}$TiO$_3$ at room temperature: a first-principles theoretical study

Manish K Niranjan

Department of Physics; Indian Institute of Technology, Hyderabad, TS, 502285, India

E-mail: manish@iith.ac.in

Abstract

Using first-principles density functional theory, the zone-center phonon spectrum, mode oscillator strengths and Raman tensor coefficients are computed for the relaxor ferroelectric Na$_{1/2}$Bi$_{1/2}$TiO$_3$ (NBT) in $R3c$ phase. Subsequently, these quantities are used to compute the Infrared (IR) reflectivity and Raman intensity spectrum. The E symmetry modes at 246, 296, 580 cm^{-1} and A_1 symmetry modes at 256, 266, 568 cm^{-1} are found to have high oscillator strengths. The computed Raman coefficients are also found to be significant for aforementioned A_1 modes. The computed IR reflectivity and Raman spectra are expected to provide benchmark first-principles theroertical results for the symmetry assignment of experimental spectra of NBT in $R3c$ phase.

1. Introduction

Complex oxides are highly promising materials for numerous technological applications [1–8]. They also exhibit wide spectrum of fascinating properties which make them attractive for interesting fundamental scientific investigations [9, 10]. Some of these properties are ferroelectricity, magnetism, high-temperature superconductivity, colossal magnetoresistance, and multiferroicity [11–13]. Over many years, lead-based piezoelectric oxides near the morphotropic phase boundary (MPB) have been extensively studied and exploited in many devices such as sensors, actuators, accelerometers, etc. However, due to toxic nature of lead, interest has been shifted towards the development of high performance lead-free and environment friendly piezoelectrics in last one decade [14–16]. In recent years, Na$_{1/2}$Bi$_{1/2}$TiO$_3$ (NBT) and its solid solutions have attracted a great deal of attention as alternative lead-free piezoelectric compounds [17–24]. The NBT is interesting relaxor perovskite (ABO$_3$) in which the A-site is equally shared by two different cations. It undergoes several phase transitions in the temperature range from 5 to 900 K [25] and shows unusual dielectric and ferroelectric properties [26, 27]. The cation disorder in the NBT at the A-site (Na/Bi) has been suggested to be the most likely reason for its relaxor behavior. The prototype high temperature cubic phase ($Pm\bar{3}m$) of NBT undergoes a phase transition to tetragonal polar phase ($P4bm$) at ~820 K [28]. The phase transition involves combination of two three-component order parameters which transform according to M_3^+ irreducible representation at the M point and the polar Γ_4^- (F_{1u}) irreducible representation at the Γ point of the Brillouin zone of parent cubic structure [29–33]. The freezing of these order parameters results in in-phase TiO$_6$-octahedra tilting ($a^0a^0a^+$) and spontaneous polarization in tetragonal structure. The tetragonal phase further undergoes a phase transition at ~593 K to polar rhombohedral phase. This phase transition can also be described using two order parameters transforming according to R_4^+ irreducible representation at the R point and the polar Γ_4^- (F_{1u}) irreducible representation at the Γ point of the Brillouin zone of cubic structure. The order parameters freezing causes equal anti-phase TiO$_6$-octahedra tilting ($a^-a^-a^-$) about all crystallographic axes and spontaneous polarization [31]. At room temperature, the NBT crystallizes in aforementioned rhombohedral structure and exhibits spontaneous polarization ($P \cong 38\ \mu C\ cm^{-2}$) along the 3-fold [111] direction and relatively a large coercive field (~70 kV cm^{-1}). Though the remnant polarization is comparable to that in prototypical ferroelectric materials, the large

coercive field in NBT makes its piezoelectric properties undesirable. Nonetheless, the piezoelectric properties of NBT and its solid solutions can be improved by cation substitution at the *A* and *B*-sites as demonstrated in several recent reports [34–36]. Significant improvement in piezoelectric behavior in NBT based solid solutions around the MPB region has also been demonstrated. Besides having important technological applications, the NBT system is also interesting for scientific investigations as the origin of its various intrinsic properties and their structure-property correlations have not been explored in detail so far. Over past several years, Infrared (IR) and Raman vibrational spectroscopic techniques have been widely used to investigate various structural and dynamical aspects in oxide systems. These techniques are particularly useful and advantageous in providing precise information of ionic configurations and local distortions in the crystal structure [37–41]. In last several years, several experimental Raman studies of single crystal and ceramic NBT have been reported [42–48]. On the other hand, except the work reported by Petzelt *et al*, no experimental IR study of NBT has been reported to the best of our knowledge [33]. Moreover, on the theoretical front, reported studies of room temperature rhombohedral phase of NBT are scarce. In particular, no theoretical study of IR and Raman intensity spectra of NBT has been reported to the best of our knowledge. In this article, we present a first-principles study of IR response and Raman intensities of NBT (*R3c* phase) within the framework of density-functional theory. In particular, we compute and analyze IR reflectivity, Raman tensor coefficients and Raman spectrum.

This article is organized as follows. Theoretical analysis is reviewed in section 2 with details of IR reflectivity and Raman intensity spectrum calculations in sections 2.1 and 2.2 respectively. The density functional computational methodology is presented in section 2.3. The results are discussed and analyzed in section 3. Finally, the conclusions are presented in section 4.

2. Theoretical details

2.1. IR response

The frequency dependent complex dielectric permittivity tensor of a material in terms of phonon mode contributions can be expressed as [49–51].

$$
\begin{aligned}
\varepsilon_{\alpha\beta}(\omega) &= \varepsilon_{\alpha\beta}^{\infty} + \sum_m \varepsilon_{m,\alpha\beta}(\omega) \\
&= \varepsilon_{\alpha\beta}^{\infty} + \frac{4\pi}{\Omega_0}\sum_m \frac{S_{m,\alpha\beta}}{\omega_m^2 - \omega^2 + i\gamma_m\omega},
\end{aligned}
\tag{1}
$$

where $\varepsilon_{\alpha\beta}^{\infty}$ is the electronic dielectric permittivity tensor, $\varepsilon_{m,\alpha\beta}$ is the contribution of *m*th IR-active phonon mode to dielectric response, $S_{m,\alpha\beta}$ is the oscillator-strength of the *m*th mode, Ω_0 is the primitive cell volume, γ_m is the damping coefficient and ω_m is the angular frequency of *m*th optical phonon mode. The oscillator strength ($S_{m,\alpha\beta}$) can be further expressed in terms of the Born effective charge tensors ($Z_{\tau,\alpha\beta}^*$) and the eigendisplacements ($U_m(\tau\beta)$) as [49]:

$$
S_{m,\alpha\beta} = \left(\sum_{\tau\alpha'} Z_{\tau,\alpha\alpha'}^* U_m^*(\tau\alpha')\right)\left(\sum_{\tau'\beta'} Z_{\tau',\beta\beta'}^* U_m(\tau'\beta')\right).
\tag{2}
$$

Furthermore, the mode effective charge ($Z_{m,\alpha}^*$) can be expressed as:

$$
Z_{m,\alpha}^* = \frac{\sum_{\tau,\beta} Z_{\tau,\alpha\beta}^* U_m(\tau\beta)}{\sqrt{\sum_{\tau,\beta} U_m^*(\tau\beta) U_m(\tau\beta)}}.
\tag{3}
$$

The eigenvectors satisfy normalization condition with the mass factor M_τ, which indicates the mass of ion τ.

$$
\sum_{\tau\beta} M_\tau U_m^*(\tau\beta) U_n(\tau\beta) = \delta_{mn}.
\tag{4}
$$

The dielectric permittivity function along the direction $\hat{\vec{q}}$ can be obtained as [49]:

$$
\varepsilon_{\hat{\vec{q}}}(\omega) = \sum_{\alpha\beta} \hat{q}_\alpha \varepsilon_{\alpha\beta}(\omega) \hat{q}_\beta.
\tag{5}
$$

As discussed in section 4, the optical phonon modes in NBT are polarized along the *z*-axis (A_1) and in the *x–y* plane (*E*). The contribution of these modes to dielectric permittivity function can be obtained using equation (5).

Finally, the reflectivity of optical radiation normal to the surface can be expressed as:

$$
R = \left|\frac{\sqrt{\varepsilon_{\hat{\vec{q}}}(\omega)} - 1}{\sqrt{\varepsilon_{\hat{\vec{q}}}(\omega)} + 1}\right|^2.
\tag{6}
$$

The electric field of the radiation is assumed to be along the optical axis $\hat{\vec{q}}$ of the crystal.

2.2. Raman spectrum

In crystals, the Raman scattering refers to the inelastic light scattering by the normal modes of vibrations. The Raman scattering intensities can be computed following theoretical background developed by G. Placzek and others. In this approach, the intensities can be expressed in terms of variations in electronic (high-frequency) dielectric permittivity $\varepsilon^\infty(\omega)$ due to phonons [52–54]. In case of single crystals, the Raman intensity associated with mode m, polarization along γ, and field along β can be expressed as [54, 55]:

$$I_{m\gamma\beta} = \frac{2\pi\hbar(\omega_i - \omega_m)^4}{c^4\omega_m[1 - \exp(-\hbar\omega_m/k_B T)]}(\alpha_{m\gamma\beta})^2, \tag{7}$$

where ω_m is the angular frequency of mth phonon mode, ω_i is the angular frequency of the incident radiation, $\hbar$ is the Plank constant, k_B is the Boltzmann constant, T is the temperature and α is the Raman susceptibility tensor defined as:

$$\alpha_{m\gamma\beta} = \frac{\sqrt{\Omega_0}}{4\pi}\sum_{\tau,\gamma}R_{m\alpha\beta}(\tau\gamma)U_m(\tau\gamma)M_\tau^{-1/2}, \tag{8}$$

where $U_m(\tau\gamma)$ is the eigenvector of the dynamical matrix, M_τ is the mass of atom τ, Ω_0 is the volume of the unit cell, $R_{m\alpha\beta}(\tau\gamma)$ is the derivative of high-frequency dielectric constant ($\varepsilon^\infty_{\alpha\beta}$) with respect to the displacement $u_m(\tau\gamma)$ of atom τ in mth mode in γ direction.

$$R_{m\alpha\beta}(\tau\gamma) = \frac{\partial\varepsilon^\infty_{\alpha\beta}(\omega_i)}{\partial u_m(\tau\gamma)}. \tag{9}$$

For powder or polycrystals, the integral intensity is averaged over the possible directions of the crystallites [52, 54]

$$G^{(0)}_m = \frac{1}{3}(\alpha_{mxx} + \alpha_{myy} + \alpha_{mzz}), \tag{10}$$

$$G^{(1)}_m = \frac{1}{2}[(\alpha_{mxy} - \alpha_{myx})^2 + (\alpha_{mxz} - \alpha_{mzx})^2 + (\alpha_{mzy} - \alpha_{myz})^2] \tag{11}$$

$$\begin{aligned} G^{(2)}_m &= \frac{1}{2}[(\alpha_{mxy} - \alpha_{myx})^2 + (\alpha_{mxz} - \alpha_{mzx})^2 + (\alpha_{mzy} - \alpha_{myz})^2] \\ &+ \frac{1}{3}[(\alpha_{mxx} - \alpha_{myy})^2 + (\alpha_{mxx} - \alpha_{mzz})^2 + (\alpha_{myy} - \alpha_{mzz})^2]. \end{aligned} \tag{12}$$

If a polarized laser beam and a scattered radiation analyzer is used, then for the backscattering and 90° geometry, the Raman intensity for the powder can be expressed as [52, 56, 57]

$$I^{poly}_{m||} \sim (\omega_i - \omega_m)^4\frac{1}{30\omega_m[1 - \exp(-\hbar\omega_m/k_B T)]}[10G^{(0)}_m + 4G^{(2)}] \tag{13}$$

$$I^{poly}_{m\perp} \sim (\omega_i - \omega_m)^4\frac{1}{30\omega_m[1 - \exp(-\hbar\omega_m/k_B T)]}[5G^{(0)}_m + 3G^{(2)}], \tag{14}$$

where $||$ and $\perp$ correspond to polarized and unpolarized light respectively. The total intensity for the mth mode can be expressed as

$$I^{poly}_{m\,Tot} = I^{poly}_{m\,||} + I^{poly}_{m\,\perp}. \tag{15}$$

Finally, the Raman spectrum can be plotted using the Lorentzian line shape as

$$I^{poly}(\omega) = \sum_m I^{poly}_m\frac{\Gamma_m}{(\omega - \omega_m)^2 + \Gamma_m^2}, \tag{16}$$

where Γ_m is the damping coefficient of the mth mode.

2.3. Computational methodology

The calculations are performed within the framework of density functional theory as implemented in the ABINIT package [58, 59]. The exchange-correlation energy is approximated within local-density approximation (LDA) [60]. The norm-conserving pseudopotentials generated using Troullier–Martins approach are used to approximate electron-ion interactions [61]. The Kohn–Sham wave functions are expanded in plane wave basis with kinetic energy cutoff of 50 Hartree. A $8 \times 8 \times 8$ Monkhorst-Pack k-point mesh is employed for the Brillouin zone sampling. The ions are relaxed until the largest force on each ion becomes less than 0.01 eV Å^{-1}. Self-consistency in calculations is achieved until the total energies are converged to 10^{-6} eV/cell. Born-effective charge tensors, zone-centered phonon frequencies and linear optical susceptibility are computed within a

Table 1. Computed (LDA) and experimental lattice constant a_o (Å), angle α (in degrees), and structural parameters of $Na_{1/2}Bi_{1/2}TiO_3$ in $R3c$ phase.

		a_0	α	$x_{Na/Bi}$	x_{Ti}	x_O	y_O	z_O
Calc.	This work	5.678	59.58	0.2740	0.0069	0.1736	0.3280	0.7395
	Ref. [48]	5.421	59.50	0.2707	0.0117	0.1827	0.3140	0.7441
Exp.	Ref. [48]	5.4987	59.80	0.2611	0.0063	0.2070	0.2866	0.7496
	Ref. [25]	5.5051	59.80	0.2627	0.0063	0.2093	0.2933	0.7496

Table 2. Computed (LDA) frequencies (cm^{-1}) and symmetry assignments of TO and LO modes in $Na_{1/2}Bi_{1/2}TiO_3$ in $R3c$ phase.
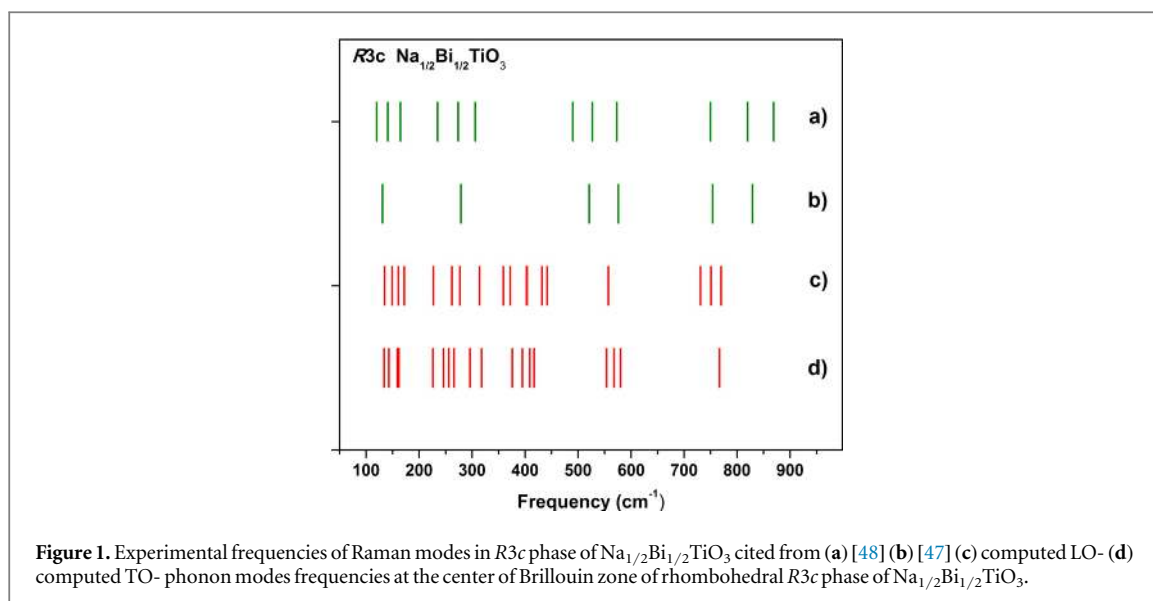
Modes	$\nu(cm^{-1})$	Modes	$\nu(cm^{-1})$
$E(TO1)$	143	$A_1(TO1)$	134
$E(LO1)$	149	$A_1(LO1)$	135
$E(TO2)$	159	$A_1(TO2)$	162
$E(LO2)$	161	$A_1(LO2)$	172
$E(TO3)$	226	$A_1(TO3)$	256
$E(LO3)$	227	$A_1(LO3)$	262
$E(TO4)$	246	$A_1(TO4)$	266
$E(LO4)$	277	$A_1(LO4)$	314
$E(TO5)$	296	$A_1(TO5)$	318
$E(LO5)$	359	$A_1(LO5)$	372
$E(TO6)$	376	$A_1(TO6)$	395
$E(LO6)$	404	$A_1(LO6)$	403
$E(TO7)$	409	$A_1(TO7)$	417
$E(LO7)$	442	$A_1(LO7)$	432
$E(TO8)$	554	$A_1(TO8)$	568
$E(LO8)$	557	$A_1(LO8)$	731
$E(TO9)$	580	$A_1(TO9)$	767
$E(LO9)$	751	$A_1(LO9)$	770

variational approach to density functional perturbation theory [59]. Finite differences are used to compute derivatives of the linear optical susceptibility with respect to atomic displacements.

3. Results and discussion

As discussed earlier, NBT crystallizes at room temperature in non-centrosymmetric rhombohedral structure with $R3c$ space group symmetry. In our calculations, the NBT unit cell consists of ten atoms, wherein Na and Bi ions are ordered in a cell doubled along [111] axis of the perovskite structure. The z axis coincides with the 3-fold [111] axis. The calculated lattice constants, angle (α) and atomic positions (x, y, z) are listed in table 1 and are in good agreement (within 1%–2%) with reported experimental and theoretical values.

The zone-center optical phonon modes of the $R3c$ phase of NBT in the absence of A-site disorder can be expressed according to irreducible representation, $\Gamma = 9A_1 \oplus 9E$ [33, 62]. However, in presence of A-site disorder, the irreducible representation is modified to $\Gamma = 4A_1 \oplus 9E \oplus 5A_2$ [33]. The optical non-degenerate A_1 and doubly degenerate E modes are polarized along the z-axis and in the x–y plane respectively. The A_1 and E optical modes are both Raman and IR active. On the other hand, non-degenerate A_2 modes are silent. The computed frequencies of transverse (TO) and longitudinal (LO) optical modes with A_1 and E symmetry are listed in table 2. Figure 1 shows a comparison of computed frequencies in the present work with reported experimental Raman mode frequencies [42, 47]. The computed values are in good agreement with previously reported experimental values. The difference between the computed and experimental mode frequencies can be partially attributed to the absence of disorder at the A-site in the theoretical model and the limitations of local density approximation in describing the exchange-correlation functional. The difference may also be due to recently reported coexistence of monoclinic CC phase with rhombohedral $R3c$ phase in the NBT at the room temperature [63–65]. This coexistences of two phases has been suggested to be due to specific chemical ordering of Na and Bi ions at the A-site in the NBT [66]. Furthermore, the low frequency mode at ~ 50 cm^{-1} in experimental Raman spectrum of NBT is suggested to be that belonging to the monoclinic CC phase. It may be noted that the computed mode frequencies correspond to temperature at 0 K whereas experimental values are obtained from room temperature (300 K) Raman spectrum. The mode frequencies are expected to decrease by

Figure 1. Experimental frequencies of Raman modes in *R3c* phase of $Na_{1/2}Bi_{1/2}TiO_3$ cited from (**a**) [48] (**b**) [47] (**c**) computed LO- (**d**) computed TO- phonon modes frequencies at the center of Brillouin zone of rhombohedral *R3c* phase of $Na_{1/2}Bi_{1/2}TiO_3$.

~3–4 cm^{-1} with the increase in temperature from 0 to 300 K. The variation of mode frequencies with temperature may be due to anharmonic contributions resulting from thermal expansion and phonon–phonon coupling [67].

As can be seen in table 2, the largest splitting between LO and TO modes (LO8-TO8 and LO9-TO9) is computed to be ~170 cm^{-1} and is indeed significant. However, the computed values of LO mode frequencies are likely to be less accurate than those for TO modes due to limitations of LDA approximation [68]. The LO-TO splitting depends on electronic dielectric permittivity which is generally overestimated in LDA approximation. As can be seen in table 2 and figure 1, the Raman modes of NBT are overlapped together and appear as four major bands in the frequency range of 130–170 cm^{-1}, 230–440 cm^{-1}, 550–580 cm^{-1} and 730–850 cm^{-1}. The computed eigenvectors reveal that Bi atoms participate only in the lowest frequency modes in the range of 134–160 cm^{-1}. High frequency modes in the range 403–770 cm^{-1} are primarily associated with the vibrations of oxygen atoms. The Na-O and Ti-O vibrations dominate in the modes in the frequency range of 160–395 cm^{-1} respectively. Next we show, the real and imaginary parts of complex dielectric permittivity function as function of frequency in figure 2. The damping constant equal to ~10 cm^{-1} is used for all modes. Figure 2 shows the primary absorption peaks lying in the frequency range of 220–430 cm^{-1} and 550–580 cm^{-1}. Further, the strongest absorption peak can be seen to be centered at ~250 cm^{-1}. The components of optical dielectric tensor (ε^{∞}) parallel and perpendicular to 3-fold [111] axis are computed to be 7.08 and 7.75. The average value of ε^{∞} comes out to be 7.52 and is obtained by taking one-third of the trace of dielectric tensor. The computed magnitude is overestimated as compared to reported experimental values ~5.62–6.71 [69]. The LDA computed values of optical dielectric tensor components are expected to be overestimated by ~ 10%. The error is due to underestimated values of bandgaps and hence screening which in turn may be attributed to lack of polarization dependence in the exchange-correlation functional [70, 71]. However, it may be noted that several quantities such as optical phonon frequency at the zone center, which may critically depend on dielectric screening, are computed to a better accuracy using LDA than the value of optical dielectric constant (ε^{∞}) [71, 72]. Using equation (1), the static dielectric tensor components parallel and perpendicular to 3-fold [111] axis are computed to be 30.2 and 36.4 respectively. The computed oscillator strengths of A_1(TO) and E(TO) modes are listed in table 3. The E symmetry modes with frequencies 246 cm^{-1}, 580 cm^{-1}, 296 cm^{-1} and A_1 symmetry modes with frequencies 568 cm^{-1}, 256 cm^{-1}, 266 cm^{-1} are found to have high oscillator strengths.

The figure 3 shows the IR reflectivity spectra calculated using equation (6). The IR spectra at normal incidence on [001] and [100] NBT surfaces are shown in figures 3(b) and (c) respectively. The average reflectivity spectrum is shown in figure 3(a). As evident, the IR spectrum exhibits characteristics patterns common to many perovskite oxides [51, 73]. As can be seen, the spectrum consists of four major bands. The low-frequency band is located below ~160 cm^{-1}. The second band consists modes with frequencies in the range ~230–450 cm^{-1}. The modes in the range of ~550–600 cm^{-1} and ~700–850 cm^{-1} form third and fourth band. The computed IR spectrum is in qualitative agreement with the experimental IR spectrum presented in [33] with regard to frequency positions as well as peak intensities. The disagreement between theoretical and experimental IR spectrum may be attributed to several factors. In equation (6), the damping factor of ~10 cm^{-1} is used for all modes. However, in case of perovskites, the damping factor may vary with mode frequencies in the range of 5–50 cm^{-1} [51]. Furthermore, all IR-active modes are used in summation in equation (6). In our calculations,
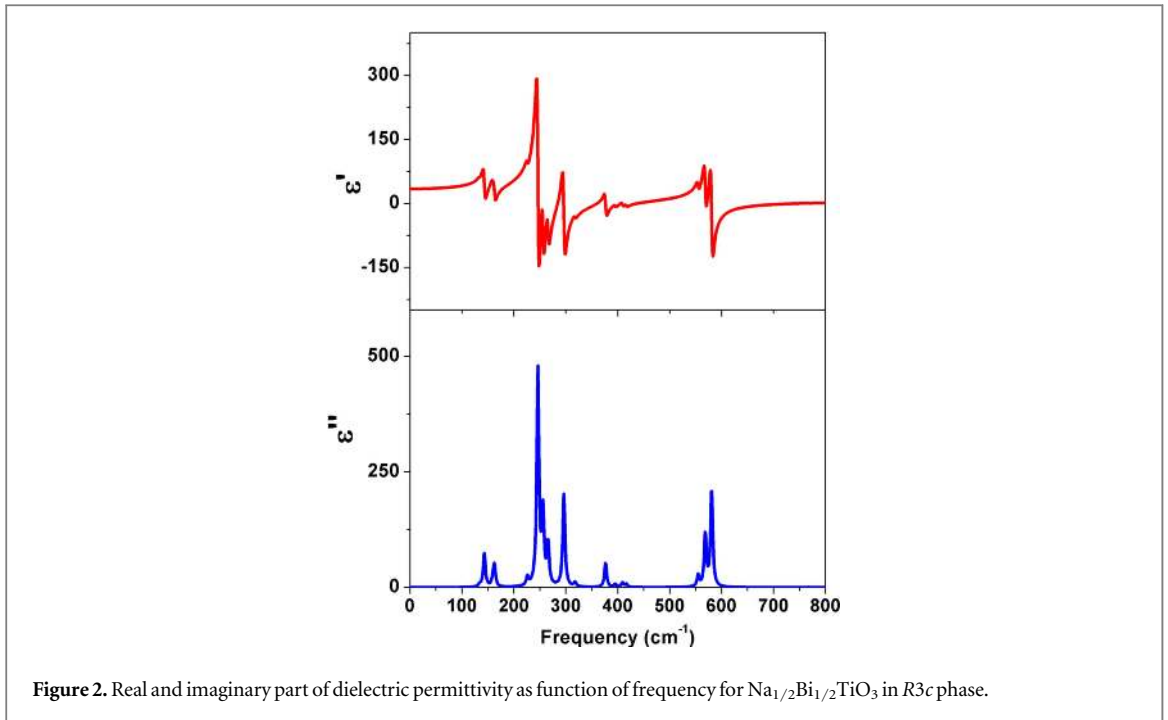
Figure 2. Real and imaginary part of dielectric permittivity as function of frequency for $Na_{1/2}Bi_{1/2}TiO_3$ in $R3c$ phase.

Table 3. Computed (LDA) values of IR oscillator strength tensor coefficients ($\times 10^{-5}a.\ u$) and Raman coefficients ($\times 10^{-5}$) of the TO modes in $Na_{1/2}Bi_{1/2}TiO_3$ in $R3c$ phase.

Modes	Oscillator strength			Raman coefficients			
	$S_{xx} = S_{yy}$	S_{zz}	Poly-crystalline	a^2	b^2	c^2	d^2
$A_1(TO1)$	0	1.48	0.99	0.48	1.84		
$E(TO1)$	11.21	0	7.47			0.47	1.22
$E(TO2)$	2.16	0	1.44			0.24	0.28
$A_1(TO2)$	0	16.34	10.89	0.18	1.62		
$E(TO3)$	4.55	0	3.03			0.15	0.81
$E(TO4)$	123.41	0	82.27			1.84	0.04
$A_1(TO3)$	0	86.3	57.53	0.75	20.93		
$A_1(TO4)$	0	50.55	33.7	5.02	18.01		
$E(TO5)$	63.46	0	42.31			2.13	4.72
$A_1(TO5)$	0	6.36	4.24	0.67	0.77		
$E(TO6)$	21.20	0	14.13			5.71	0.58
$A_1(TO6)$	0	5.85	3.90	1.92	2.18		
$E(TO7)$	4.47	0	2.98			1.57	4.49
$A_1(TO7)$	0	6.52	4.35	0.09	7.72		
$E(TO8)$	14.67	0	9.78			1.61	0.07
$A_1(TO8)$	0	137.55	91.7	11.09	76.97		
$E(TO9)$	131.44	0	87.63			6.90	7.13
$A_1(TO9)$	0	0.71	0.47	0.03	0.75		

the A_2 modes, which are IR silent, are not identified due to absence of disorder at the A-site. On the experimental front, it is generally difficult to observe full IR spectrum as the modes having low oscillator strength may not be detected. Furthermore, modes which are close in frequency and are heavily damped may not be resolved unambiguously. Thus, only few oscillators are generally required to fit the experimental spectrum.

Next, we compute Raman tensor coefficients and Raman intensity spectrum. The Raman susceptibility tensors of A_1 and E modes are given as [61, 74]:

$$A_1(z) = \begin{bmatrix} a & \cdot & \cdot \\ \cdot & a & \cdot \\ \cdot & \cdot & b \end{bmatrix}, E(x) = \begin{bmatrix} c & \cdot & d \\ \cdot & -c & \cdot \\ d & \cdot & \cdot \end{bmatrix}, E(y) = \begin{bmatrix} \cdot & -c & \cdot \\ -c & \cdot & d \\ \cdot & d & \cdot \end{bmatrix}. \quad (17)$$

The absolute values of computed Raman coefficients are listed in table 3. As can be seen, the Raman coefficient magnitudes are significant for A_1 symmetry modes with frequencies 256, 266 and 568 cm^{-1}. The Raman spectrum of polycrystal NBT computed using equations (13)–(16) and damping constant (Γ_m)
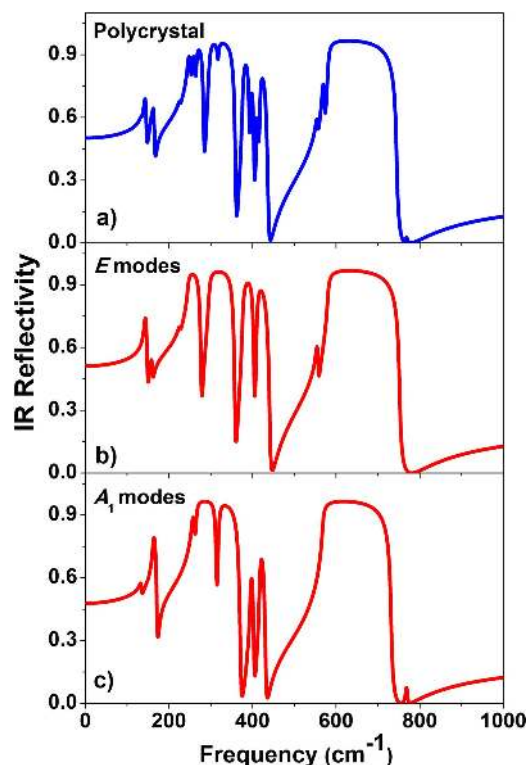
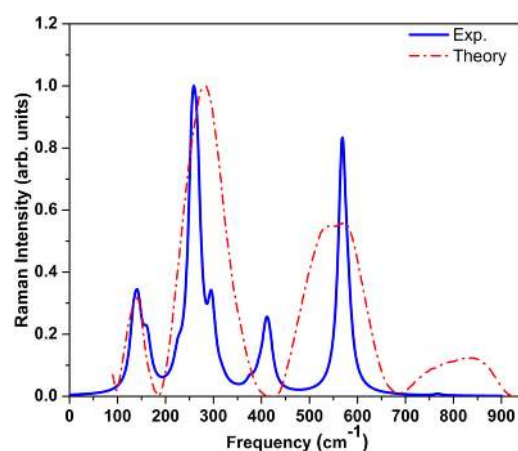**Figure 3.** Computed IR reflectivity spectra for $Na_{1/2}Bi_{1/2}TiO_3$ in $R3c$ phase.

Figure 4. Theoretical (solid blue) and experimental (dash-dot red) [48, 75] Raman intensity spectra of polycrystalline $Na_{1/2}Bi_{1/2}TiO_3$ in $R3c$ phase.

$\sim$10 cm^{-1} is shown in figure 4 and compared with the experimental spectrum [48, 75]. Further, the computed spectra of NBT in $x(zz)y$ and $z(xy)\bar{z}$ configurations and their average are shown in Figures 5(a)–(c). It may be noted that the pure $A_1(TO)$ and $E(TO)$ modes can be detected in $x(zz)y$ and $z(xy)\bar{z}$ configurations respectively. The relative Raman intensities of phonon modes are listed in table 4. As can be seen in figure 4 and figure 5, the intensity peaks are centered at mode frequencies 140, 262, 296, 376, 408 and 569 cm^{-1}. Figure 4 shows significant higher intensity for A_1 modes ($x(zz)y$ configuration) centered at 262 and 569 cm^{-1}. Though the computed Raman spectrum is in reasonable agreement with experimental spectrum [42, 47, 48], several factors may contribute to differences between them. For instance, the observed Raman spectra can be quite sensitive to the degree of cation disorder which may result in excitations of phonons at wavevectors in the entire Brillouin zone [76]. Additional Raman lines in the experimental spectrum can also be due to nanoscale chemically ordered domains in disordered matrices of oxides. Furthermore, as mentioned earlier, the
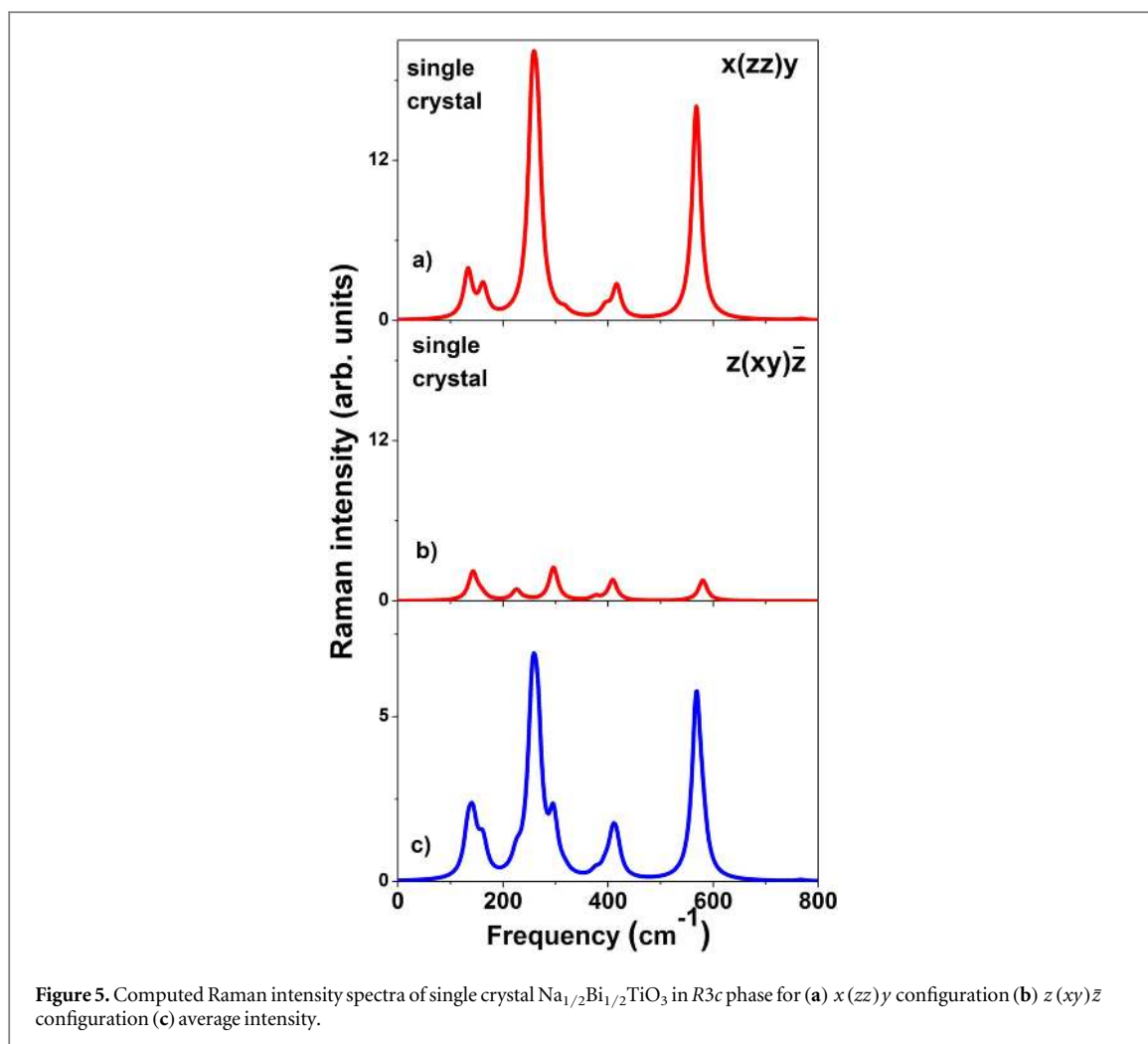
Figure 5. Computed Raman intensity spectra of single crystal $Na_{1/2}Bi_{1/2}TiO_3$ in $R3c$ phase for (**a**) $x(zz)y$ configuration (**b**) $z(xy)\bar{z}$ configuration (**c**) average intensity.

Table 4. Computed (LDA) and experimental [48, 75] relative Raman intensities of phonon modes in $Na_{1/2}Bi_{1/2}TiO_3$ in $R3c$ phase.

	Theory			Exp.	
Modes	$\nu(cm^{-1})$	I/I_0	Modes	$\nu(cm^{-1})$	I/I_0
A_1	134	0.27			
E	143	0.22			
E	159	0.05			
A_1	162	0.13			
E	226	0.08			
E	246	0.10			
A_1	256	0.66	—	246	0.51
A_1	266	0.87	—	285	1.00
E	296	0.26			
A_1	318	0.05			
E	376	0.24	—	323	0.31
A_1	395	0.11			
E	409	0.15			
A_1	417	0.10	—	484	0.17
E	554	0.05			
A_1	568	1.00	—	576	0.82
E	580	0.25			
A_1	767	0.01	—	756	0.12
			—	831	0.14

coexistence of monoclinic *CC* phase with rhombohedral *R*3c phases in NBT at room temperature may also contribute to additional lines in the experimental Raman spectrum.

4. Conclusions

The oscillator strengths of zone-center phonon modes, Raman tensor components, IR reflectivity and Raman intensity spectrum are computed for room temperature *R*3c phase of relaxor ferroelectric $Na_{1/2}Bi_{1/2}TiO_3$ (NBT) with in the framework of first-principles density functional theory. The *E* symmetry modes with frequencies 246, 296, 580 cm^{-1} are found to have high oscillator strength. Further, the A_1 modes at 256, 266, 568 cm^{-1} are found to have high oscillator strengths as well as high values of Raman coefficients. The computed IR reflectivity and Raman spectra can be used as benchmark first-principles theroretical results for the symmetry assignment of experimental spectra of NBT in *R*3c phase. The present work is expected to further stimulate theoretical and experimental studies of IR and Raman response of NBT.

Acknowledgments

References

[1] Scott J F 2007 Applications of modern ferroelectrics *Science* **315** 954
[2] Bibes M, Villlegas J E and Barthélémy A 2011 Ultrathin oxide films and interfaces for electronicsand spintronics *Adv. Phys.* **60** 5–84
[3] Manhart J and Schlom D G 2010 Oxide interfaces-an opportunity for electronics *Science* **327** 1607
[4] Heber J 2009 Enter the oxides *Nature* **459** 28
[5] Cen C, Thiel S, Mannhart J and Levy J 2009 Oxide nanoelectronics on demand *Science* **323** 1026
[6] Rijnders G and Blank D H A 2008 An atomic force pencil and eraser *Nat. Mater.* **7** 270
[7] Scott J F 2007 Multiferroic memories *Nat. Mater.* **6** 256
[8] Tsymbal E Y and Kohlstedt H 2006 Tunneling across a ferroelectric *Science* **313** 181
[9] Tokura Y and Nagaosa N 2000 Orbital physics in transitional metal oxides *Science* **288** 462
[10] Dagotto E 2005 Complexity in strongly correlated electronic systems *Science* **309** 257
[11] Eerenstein W, Mathur N D and Scott J F 2006 Multiferroic and magnetoelectric materials *Nature* **442** 759
[12] Mostovoy M 2010 A whirlwind of opportunities *Nat. Mater.* **9** 188
[13] Reyren N, Thiel S, Caviglia A D, Kourkoutis L F, Hammerl G *et al* 2007 Superconducting interfaces between insulating oxides *Science* **317** 1196
[14] Saito Y, Takao H, Tani T, Nonoyama T, Takatori K *et al* 2004 Lead free peizoceramics' *Nature* **432** 84
[15] Cross E 2004 Lead free at last *Nature* **432** 24
[16] Rodel J, Jo W, Seifert K T P, Anton E-M, Granzow T *et al* 2009 Perspective on the developmentof lead-free piezoceramics *J. Am. Ceram. Soc.* **92** 1153–77
[17] Chiang Y-M, Farrey G W and Soukhojak A N 1998 Lead-free high-strain single-crystal piezoelectrics in the alkaline–bismuth–titanate perovskite family *Appl. Phys. Lett.* **73** 3683
[18] Siny I G, Tu C-S and Schimidt V H 1995 Critical acoustic behavior of therelaxor ferroelectric $Na_{1/2}Bi_{1/2}TiO_3$ in the intertransition region *Phys. Rev.* B **51** 5659
[19] Kriesel J, Glazer A M, Bouvier P and Lucazeau G 2001 High-pressure Raman study of a relaxorferroelectric: The $Na_{1/2}Bi_{1/2}TiO_3$ perovskite *Phys. Rev.* B **63** 174106
[20] Daniels J E, Jo W, Rodel J and Jones J L 2009 Electric-field-induced phase transformation at alead-free morphotropic phase boundary: case study in a 93%($Bi_{1/2}Na_{1/2}$)TiO_3–7%$BaTiO_3$ piezoelectric ceramic *Appl. Phys. Lett.* **95** 032904
[21] Jo W, Granzow T, Aulbach E, Rodel J and Damjanovic D 2009 Origin of the large strainresponse in ($K_{1/2}Na_{1/2}$)NbO_3-modified ($Bi_{1/2}Na_{1.2}$)TiO_3–$BaTiO_3$ lead-free piezoceramics' *J.Appl. Phys.* **105** 094102
[22] Hiruma Y, Nagata H and Takenaka T 2009 Thermal depoling process and piezoelectric propertiesof bismuth sodium titanate ceramics *J. Appl. Phys.* **105** 084112
[23] Shuvaeva V A, Zekria D, Glazer A M, Jiang Q, Weber S M *et al* 2005 Local structure of thelead-free relaxor ferroelectric (K_xNa_{1-x})$_{1/2}Bi_{1/2}TiO_3$ *Phys. Rev.* B **71** 174114
[24] Kreisel J, Bouvier P, Dkhil B, Thomas P A, Glazer A M *et al* 2003 High-pressure x-rayscattering of oxides with a nanoscale local structure: application to $Na_{1/2}Bi_{1/2}TiO_3$ *Phys. Rev.* B **68** 014113
[25] Jones G O and Thomas P A 2002 Investigation of the structure and phase transitions in the novelA-site substituted distorted perovskite compound $Na_{1/2}Bi_{1/2}TiO_3$ *Acta Cryst.* B **58** 168–78
[26] Suchanicz J 1998 The low-frequency dielectric relaxation $Na_{1/2}Bi_{1/2}TiO_3$ ceramics *Mater. sci. Eng.:* B **55** 114–8
[27] Park S-E, Chung S-J and Kim I-T 1996 Ferroic phase transitions in $Na_{1/2}Bi_{1/2}TiO_3$ crystals *J. Am. Ceram. Soc.* **79** 1290
[28] Jones G O and Thomas P A 2000 The tetragonal phase of $Na_{1/2}Bi_{1/2}TiO_3$—a new variant ofperovskite structure *Acta Cryst.* B **56** 426
[29] Dvorak V 1963 Group analysis of lattice vibrations of cubic perovskites ABO_3 *Phys. Status Solidi* **3** 2235
[30] Aleksandrov K S and Bartolome J 2001 Structural distortions in families of perovskite-like crystals *Phase Transit.* **74** 255
[31] Stokes H T, Kisi E H, Hatch D M and Howard C J 2002 Group-theoretical analysis ofoctahedral tilting in ferroelectric perovskite *Acta Cryst.* B **58** 934
[32] Vakhrushev S B, Isupov V A, Kvyatkovsky B E, Okuneva N M, Pronin I P *et al* 1995 Phase transitions and soft modes in sodium bismuth titanate *Ferroelectrics* **63** 153

[33] Petzelt J *et al* 2004 Infrared, Raman and high-frequency dielectric spectroscopy and thephase transitions in Na$_{1/2}$Bi$_{1/2}$TiO$_3$ *J. Phys. Condens. Matter* **16** 2719–31

[34] Hiruma Y *et al* 2008 Large electrostrain near the phase transition temperature of Na$_{1/2}$Bi$_{1/2}$TiO$_3$ –SrTiO$_3$ ferroelectric ceramics *Appl. Phys. Lett.* **92** 262904

[35] Lei N, Zhu M, Yang P, Wang L, Wang L *et al* 2011 Effect of lattice occupation behaviorof Li$^+$ cations on microstructure and electrical properties of (Bi$_{1/2}$Na$_{1/2}$)TiO$_3$-basedlead-free piezoceramics *J. Appl. Phys.* **109** 054102

[36] Aksel E, Forrester J S, Kowalski B, Deluca M, Damjanovic D *et al* 2012 Structure andproperties of Fe-modified Na$_{1/2}$Bi$_{1/2}$TiO$_3$ at ambient and elevated temperature *Phys. Rev. B* **85** 024121

[37] Taniguchi H, Soon H P, Shimizu T, Moriwake H, Shan Y J *et al* 2011 Mechanism forsuppression of ferroelectricity in Cd$_{1-x}$Ca$_x$TiO$_3$ *Phys. Rev. B* **84** 174106

[38] Dias A, Khalam L A, Sebastian M T, Paschoal C W A and Moreira R L 2006 'Chemical substitution in Ba(RE$_{1/2}$Nb$_{1/2}$)O$_3$ (RE = La, Nd, Sm, Gd, Tb, and Y)microwave ceramics and its influence on the crystal structure and phonon modes *Chem. Mater.* **18** 214–20

[39] Zhang W, Wang Z and Chen X M 2011 Crystal structure evolution and local symmetry ofperovskite solid solution Ba[(Fe$_{1/2}$Nb$_{1/2}$)$_{1-x}$Ti$_x$]O$_3$ investigated by Raman spectra *J. Appl. Phys.* **110** 064113

[40] Colomban P and Slodczyk A 2009 Raman intensity: an important tool to study the structure andphase transitions of amorphous/crystalline materials *Opt. Mater.* **31** 1759

[41] Slodczyk A and Colomban P 2010 Probing the nanodomain origin and phase transition mechanismsin (un)poled PMN-PT single crystals and textured ceramics *Materials* **3** 5007

[42] Siny I G, Husson E, Beny J M, Lushnikov S G, Rogacheva E A *et al* 2000 Raman scatteringin the relaxor-type ferroelectric Na$_{1/2}$Bi$_{1/2}$TiO$_3$ *Ferroelectrics* **248** 57

[43] Kreisel J, Glazer A M, Jones G, Thomas P A, Abello L *et al* 2000 An x-ray diffraction and Raman spectroscopy investigation of A-site substituted perovskite compounds: the(Na$_{1-x}$K$_x$)$_{1/2}$Bi$_{1/2}$TiO$_3$ solid solution *J. Phys.:Condens. Matter* **12** 3267

[44] Kreisel J, Glazer A M, Bouvier P and Lucazeau G 2001 High-pressure Raman study of a relaxorferroelectric: The Na$_{1/2}$Bi$_{1/2}$TiO$_3$ perovskite *Phys. Rev. B* **63** 174106

[45] van Eerd B W, Damjanovic D, Klein N, Setter N and Trodahl J 2010 Structuralcomplexity of Na$_{1/2}$Bi$_{1/2}$TiO–BaTiO$_3$ as revealed by Raman spectroscopy *Phys. Rev. B* **82** 104112

[46] Rout D, Moon K S, Kang S J L and Kim I W 2010 Dielectric and Raman scattering studiesof phase transitions in the (Na$_{1/2}$Bi$_{1/2}$TiO$_3$)–(SrTiO$_3$) system *J. Appl. Phys.* **108** 084102

[47] Suchanicz J, -Sumara I J and Kruzina T V 2011 Raman and infrared spectroscopy of Na$_{1/2}$Bi$_{1/2}$TiO$_3$—BaTiO$_3$ ceramics *J. Electroceramics* **27** 45–50

[48] Niranjan M K, Karthik T, Asthana S, Pan J and Waghmare U V 2013 Theoretical andexperimental investigation of Raman modes, ferroelectric and dielectric properties ofrelaxor Na$_{1/2}$Bi$_{1/2}$TiO$_3$ *J. Appl. Phys.* **113** 194106

[49] Gonze X and Lee C 1997 Dynamical matrices, born effective charges, dielectric permittivitytensors, and interatomic force constants from density-functional perturbation theory *Phys. Rev. B* **55** 10355

[50] Fox M 2010 *Optical Properties of Solids* 2nd edn (Oxford: Oxford university Press)

[51] Zelezny V, Cockayne E, Petzelt J, Limonov M F, Usvyat D E *et al* 2002 Temperaturedependence of infrared-active phonons in CaTiO$_3$: a combined spectroscopic and first-principles study *Phys. Rev. B* **66** 224303

[52] Placzek G 1934 *Handbuch der Radiologie* vol 6 (Leipzig: Akademische Verlagsgesellschaft) p 208

[53] Long D A 2002 *The Raman Effect: A Unified Treatment of the Theory of Raman Scatteringby Molecules* (Chichester: Willey)

[54] Prosandeev S A, Waghmare U, Levin I and Maslar J 2005 First-order Raman spectraof AB'$_{1/2}$B'$_{1/2}$O$_3$ double perovskite *Phys. Rev. B* **71** 214307

[55] Umari P and Pasquarello A 2003 First-principles analysis of the Raman spectrum of vitreoussilica: comparison with the vibrational density of states *J. Phys. Condens. Matter* **15** S1547

[56] Hayes W and Loudon R 1978 *Scattering of Light by Crystals* (New York: Wiley) p 113

[57] Hamaguchi H-O 1985 The resonance effect and depolarization in vibrational Raman scattering *Adv. Infrared Raman Spectrosc.* **12** 273

[58] Kohn W and Sham L J 1965 Self-consistent equations including exchange-correlation effects *Phys. Rev.* **140** A1133

[59] Gonze X, Amadon B, Anglade P-M, Beuken J-M, Bottin F *et al* 2009 ABINIT : first-principles approach to material and nanosystem properties *Comput. Phys. Commun.* **180** 2582–615

[60] Ceperley D M and Alder B J 1980 Ground state of the electron gas by a stochastic method *Phys. Rev. Lett.* **45** 566–9

[61] Troullier N and Martins J L 1991 Efficient pseudopotentials for plane-wave calculations *Phys.Rev. B* **43** 1993

[62] Rousseau D L, Bauman R P and Porto S P S 1981 Normal mode determination in crystals *J. Raman Spec.* **10** 253

[63] Aksel E, Forrester J S, Jones J L, Thomas P A, Page K *et al* 2011 Monoclinic structureof polycrystalline Na$_{1/2}$Bi$_{1/2}$TiO$_3$ *Appl. Phys. Lett.* **98** 152901

[64] Rao B N, Datta R, Chandrashekaran S S, Mishra D K, Sathe V *et al* 2013 Local structuraldisorder and its influence on the average global structure and polar properties inNa$_{1/2}$Bi$_{1/2}$TiO$_3$ *Phys. Rev. B* **88** 224103

[65] Gorfman S and Thomas P A 2010 Evidence for a non-rhombohedral average structure in the leadfree piezoelectric material Na$_{1/2}$Bi$_{1/2}$TiO$_3$ *J. Appl. Crystallogr.* **43** 1409

[66] Pan J, Niranjan M K and Waghmare U V 2016 Aliovalent cation ordering, coexisting structuresand relaxor behavior of lead-free ferroelectric Na$_{1/2}$Bi$_{1/2}$TiO$_3$: first-principles theoreticalanalysis *J. App. Phys.* **119** 124102

[67] Kim Y, Chen X, Wang Z, Shi J, Miotkowski I *et al* 2012 Temperature dependence of Raman-active optical phonons in Bi$_2$Se$_3$ and Sb$_2$Te$_3$ *Appl. Phys. Lett.* **100** 071907

[68] Rabe K M, Ahn C H and Triscone J-M (ed) *Phys. Ferroelectrics* (Berlin: Springer) 2007

[69] He C, Yi X, Wu T, Wang J, Zhu K *et al* 2014 Wavelength dependence of refractive index inlead-free Na$_{1/2}$Bi$_{1/2}$TiO$_3$ –BaTiO$_3$ single crystals *Opt. Mater.* **36** 2023

[70] Gonze X, Ghosez P and Godby R W 1995 Density-polarization functional theory of the response of a periodic insulating solid to an electric field *Phys. Rev. Lett.* **74** 4035

[71] Baroni S and Resta R 1986 Ab-initio calculation of the macroscopic dielectric constant in silicon' *Phys. Rev. B* **33** 7017

[72] Resta R 1983 Local-field effects and phonon screening in polar semiconductors *Phys. Rev. B* **27** 3620

[73] Perry C H, Khanna B N and Rupprecht G 1964 Infrared studies of perovskite titanates *Phys.Rev.* **135** A408

[74] Kroumova E, Aroyo M I, Perez-Mato J M, Kirov A, Capillas C *et al* 2003 Bilbaocrystallographic server : useful databases and tools for phase-transition studies *Phase Transit.* **76** 155

[75] Karthik T, Niranjan M K and Asthana S in preparation

[76] Siny I G, Katiyar R S and Bhalla A S 2000 Raman scattering in ferroelectricrelaxor perovskite and related thin films *Ferroelectr. Rev.* **2** 51